

Validation of the active optics on Nordic Optical Telescope

Vincent BELMONT

March 16, 2000

Acknowledgement

I would like to acknowledge H. Schwarz astronomer in charge of the Nordic Optical Telescope, who accepted me in the team he is directing on La Palma. I acknowledge also M. Andersen, my supervisor for his availability in the difficult condition he experienced during this summer, for his numerous advice, and his great help for writing this report. A special thanks also to L.Freyhammer for the help he gives me in numerous occasion (and for having enduring me as a roommate for 6 long months). Thank you to H. Khoronen who translated my report in good english, and to all the team for their friendship, and their availability, especially to C.Moreno who had to handle all the problems I had with my computer.

Contents

| | | |
|----------|--|-----------|
| 1 | Telescope alignment | 5 |
| 1.1 | Alignment of the lateral supports | 5 |
| 2 | Wavefront sensing | 9 |
| 2.1 | Korhonen-Hartmann wavefront sensor | 9 |
| 2.1.1 | Principle | 9 |
| 2.1.2 | Build-in wavefront sensor | 11 |
| 2.2 | Curvature sensing | 13 |
| 3 | Results | 16 |
| 3.1 | Wavefront sensing to active optics relation | 16 |
| 3.1.1 | Active optics of the NOT | 16 |
| 3.1.2 | Active optics to curvature sensing relation | 17 |
| 3.1.3 | The ALFOSC Korhonen-Hartmann WFS | 23 |
| 3.1.4 | Reduction of ALFOSC WFS measurements | 23 |
| 3.1.5 | Active optics to ALFOSC WFS relation | 23 |
| 3.1.6 | Active optics to build-in WFS relation | 24 |
| 3.2 | Behavior of the telescope optical aberrations | 25 |
| 3.3 | Altitude dependence of the aberrations | 27 |
| A | Manual for aligning the telescope | 33 |
| A.1 | required tools | 33 |
| A.2 | Alignment at zenith. | 34 |
| A.2.1 | Alignment of M1. | 34 |
| A.2.2 | Alignment of M2. | 36 |
| A.2.3 | Alignment on sky, pointing and active optics. | 37 |
| A.3 | Alignment away from zenith. (to be done) | 37 |
| B | Manual for aligning the build-in wavefront sensor | 38 |
| B.1 | Required tools | 38 |
| B.2 | Internal alignment | 38 |
| B.3 | Alignment with respect to the telescope | 39 |
| C | Programming | 40 |
| D | Beam splitter prism data and drawings | 49 |

Introduction

The Nordic Optical Telescope (NOT), a 2.56 m telescope, at the "Observatorio del Roque de los Muchachos" on La Palma, the Canary island, was built with an active optics system. But this system had always been used in a passive way (it is a bit a pity for an "active" optics system), with semi-permanent settings applied on the bellows to correct the main aberrations at zenith position (coma, spherical, astigmatism, triangular coma, quadratic astigmatism). The aim of this project, was to validate this active optics system, in order to make routine use of it possible. This means a preliminary phase of measuring the state of the telescope alignment, and eventually correct this, in order to start on a clear, well defined basis. Then we will have to compare different wavefront sensors, in order to verify the validity of the measurements that we will take with them. When all this preliminary work is done, we have to measure the output wavefront of the telescope in several nights. This will give us a clear idea of the long term behavior of the optic. We also have to measure the dependence of aberrations with altitude of the telescope, and establish a relationship between wavefront sensor Measurements, and Zernikes of the telescope active optics. On the basis of the results arising from these investigations, it can be considered which improvements to the active optics system should be implemented.

Chapter 1

Telescope alignment

When working as an opticians in a telescope, it is a good idea to know how the telescope is aligned. Indeed, one can't expect to align this kind of optics as one would do with a small optical system on an optical bench. In practice the opto-mechanical support system does not in it self provide reliable reference points. For this reason the telescope had never been properly aligned, as the alignment procedures relied on mechanical referencing. Because the NOT is an alt-az telescope, it has an instrument rotator, which compensates for field rotation while tracking on a target. This gives (two times) four degrees of freedom, shift and tilt of the main mirror and secondary mirror respectively, disregarding the direction of tilt and displacement. These four degrees of freedom can give rise to four errors in the alignment of the telescope:

- a) misalignment coma,
- b) focal plane tilt (corresponding to the optics system not being coaxial with the rotator axis)
- c) focal plane decenter
- d) exit pupil decenter

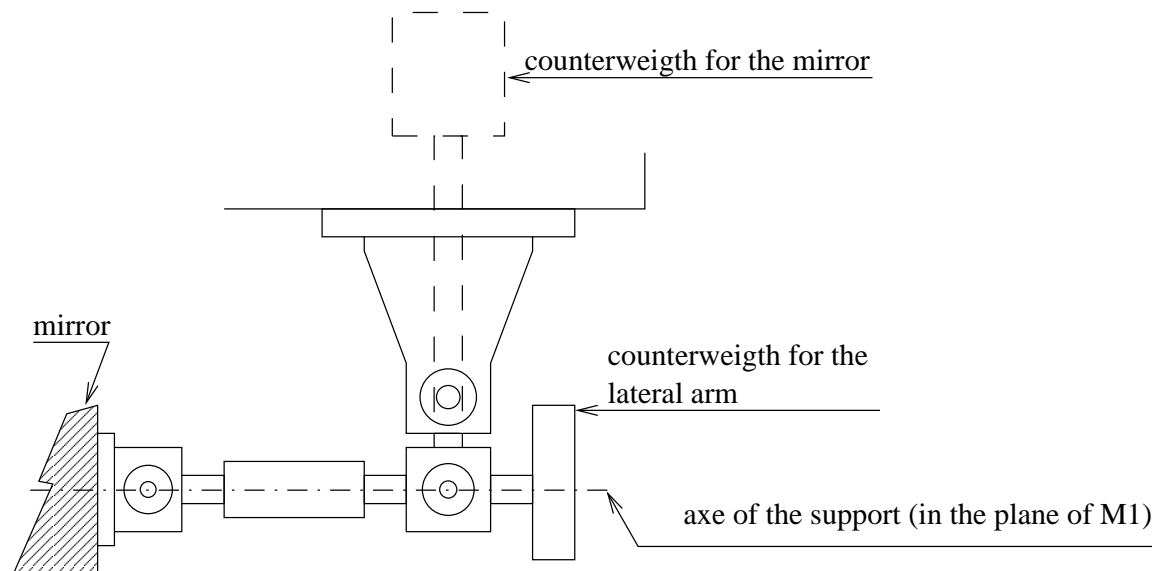
During 1997-98 several attempts were made to align the telescope optics, but it was only with the alignment of December 1998, where the procedure described in appendix 1 was used, that a good result was reached. This alignment relied on the optical figure being coaxial with the circumference of the mirror. According to T. Korhonen, coaxiality was to within 0.05mm. As was discovered after the last alignment, a misalignment error remained, corresponding to the figure of one or the mirrors to be decentered with respect to the circumference by slightly less than 1mm. This was corrected by tilting of M2, mainly resulting in a small decenter of the exit pupil.

1.1 Alignment of the lateral supports

The lateral support system for the primary mirror is designed to apply zero axial forces on the mirror at all altitudes. To fulfill this condition the arms of the supports

must be in the same plane as the mirror (see figure 1.1). If this is not really the case,

Figure 1.1: lateral support of the primary mirror



this means deformation of the mirror figure, with aberrations as function of zenith distance as a result. A force of a few Newton is enough to influence the shape of the mirror. Indeed, the rim of the mirror is about the worst place to exert forces. Some precedent investigations revealed that the supports were out of level by 0.75mm. That was far too much, since the allowed misalignment of the lateral supports is in the order of a few thousands of a radian, corresponding to an error in level of the bearings of $\approx 0.25\text{m}$, or 2 Newton or 0.2 % of the support force. The reason for the 'out of level' errors in the supports is general skewnesses of the mechanical structure. At the time of installation of the telescope no attempt had been made to compensate for these errors. Indeed, one can also see that the numbers written on the supports do not match with the ones written on the rim of the mirror. Due to various reasons, especially a need to modify the special tool we used to do this measurement (an aluminum support for the spirit level which can be mounted on the lateral supports) because of the impossibility of getting access to 2 supports, the alignment of the lateral support wasn't completed when I arrived in April 99. I then did a series of measurements on the supports, with the improved tool. Even with this modification of the tool, the measurement of the supports which were unreachable (#14 and #15) remains difficult, and the standard deviation of the measurements of these 2 supports is bigger than for the rest of the supports (about 0.05 mm for #14 for an average of 0.02 mm for the others). The first set of measurements confirmed the precedent conclusion. In other words, even if the out of level of the bearings were in the range of -0.55 mm to 0.4 mm, very few of them were out of level by more than -0.2 mm. In order to correct the level of all the supports with shims, one should have lower M1 by 0.55 mm, but this value would have been too big, and then

Table 1.1: Alignment of lateral supports.

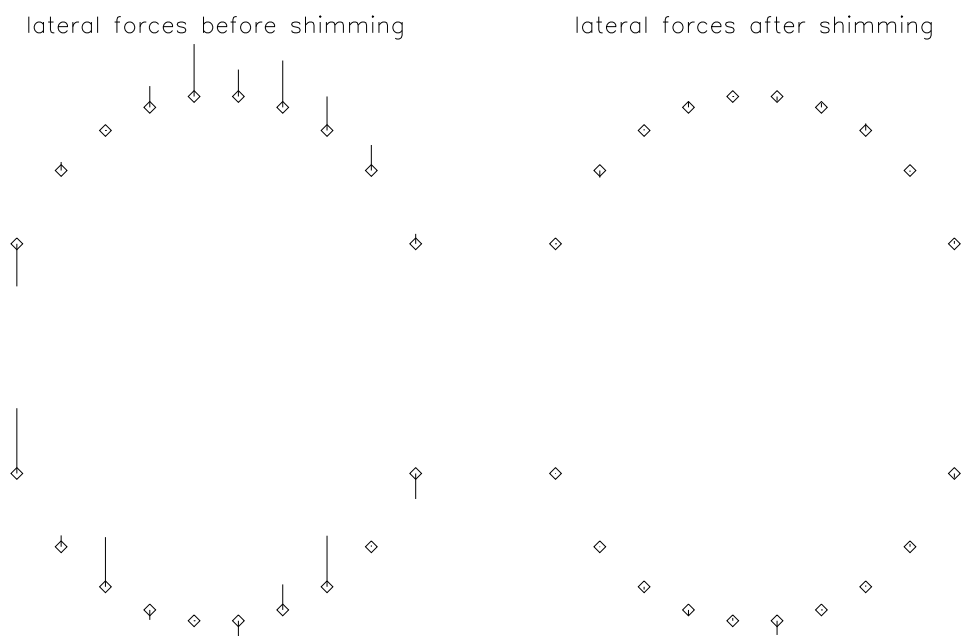
| support number | 1st meas. | 2nd meas. | 3rd meas. | average | shim thickness | value after shimming |
|----------------|-----------|-----------|-----------|---------|----------------|----------------------|
| 1 | 0.09 | 0.03 | 0.04 | 0.05 | 0.00 | 0.03 |
| 2 | 0.24 | 0.21 | 0.20 | 0.22 | 0.20 | -0.01 |
| 3 | 0.32 | 0.38 | 0.36 | 0.36 | 0.35 | 0.07 |
| 4 | 0.45 | 0.46 | 0.46 | 0.45 | 0.45 | 0.04 |
| 5 | 0.26 | 0.21 | 0.23 | 0.23 | 0.20 | -0.04 |
| 6 | 0.50 | 0.51 | 0.51 | 0.51 | 0.50 | 0.00 |
| 7 | 0.20 | 0.23 | 0.23 | 0.22 | 0.20 | 0.05 |
| 8 | 0.00 | -0.01 | -0.03 | -0.01 | 0.00 | 0.01 |
| 9 | 0.08 | 0.04 | 0.07 | 0.06 | 0.00 | -0.06 |
| 10 | -0.41 | -0.32 | -0.34 | -0.36 | -0.35 | 0.00 |
| 11 | 0.62 | 0.59 | 0.61 | 0.61 | 0.60 | 0.00 |
| 12 | 0.11 | 0.09 | 0.12 | 0.11 | 0.10 | 0.00 |
| 13 | 0.47 | 0.49 | 0.47 | 0.48 | 0.50 | -0.03 |
| 14 | -0.09 | 0.03 | -0.08 | -0.05 | 0.00 | -0.05 |
| 15 | 0.00 | -0.04 | -0.01 | -0.02 | 0.00 | 0.03 |
| 16 | -0.15 | -0.16 | -0.17 | -0.16 | -0.15 | -0.13 |
| 17 | 0.24 | 0.24 | 0.26 | 0.25 | 0.25 | 0.00 |
| 18 | 0.49 | 0.49 | 0.50 | 0.49 | 0.5 | 0.01 |
| 19 | 0.01 | 0.08 | 0.01 | 0.04 | 0.00 | 0.03 |
| 20 | -0.24 | -0.20 | -0.20 | -0.22 | -0.2 | -0.04 |

we decided to lower the mirror by only 0.2 mm, and machine again the few support which were still out of level with a negative value. The table 1.1 gives the sets of measurements done after having lowered M1¹, the average of this measurements, the value retained for the thickness of the shims (negatives thickness are for the supports to be machine), and then the value after shimming ². figure 1.2 gives a more visual idea of the improvement made by shimming the lateral supports. The diamonds represent the fixating point of each support on the rim of the mirror, and the vectors, the direction and amplitude of the forces applied on the mirror by these supports.

¹in this measurement a few were obviously wrongs, so I remade them later and replaced the corresponding value in the table.

²support #16 have not been machined yet when i did this last set of measurement

Figure 1.2: Forces applied by the lateral supports before, and after shimming



Chapter 2

Wavefront sensing

In order to analyze the functionality of the active optics, we have to know the shape of the wavefront. The Zernikes polynomials is one way of representing the wavefront aberrations on a unit circle aperture with a series of hortonormal function. They are described like this:

$$\Phi(\rho, \theta) = \frac{1}{\sqrt{2}} \sum_{n=0}^{\infty} A_{n0} R_n^0 \left(\frac{\rho}{R'} \right) + \sum_{n=1}^{\infty} \sum_{m=1}^n [A_{nm} \cos m\theta + B_{nm} \sin m\theta] R_n^m \left(\frac{\rho}{R'} \right)$$

where

$$R_n^m \left(\frac{\rho}{R'} \right) = \sum_{s=0}^{\frac{n-m}{2}} (-1)^s \frac{(n-s)!}{s! \left(\frac{n+m}{2} - s \right)! \left(\frac{n-m}{2} - s \right)!} \left(\frac{\rho}{R'} \right)^{n-2s} ; n - m \text{ even}$$

Many differents methods actually exist to estimate the coefficients of this polynomials for a particular wavefront. To do it, we will use two methods: the Korhonen-Hartmann, and the curvature sensing method.

Two wavefront sensors are currently available at the NOT. Both are Korhonen-Hartmann wavefront sensors. The first one (Build-in wavefront sensor) had been build by T. Korhonen, who invented this technique. It was first used for testing the mirror during manufacturing at the Turola optical laboratory, Finland, and was later installed at the telescope during the commissioning phase. The second one (*ALFOSC* wavefront sensor), is a dioptric modification of the Korhonen-Hartmann test implemented by my supervisor M. Andersen. A third one working on the curvature sensing principle, is to be installed in the standby camera (*StanCam*).

2.1 Korhonen-Hartmann wavefront sensor

2.1.1 Principle

The Korhonen Hartman wavefront sensor had been first developed for testing the quality of big astronomical mirrors during their construction [1]. Indeed the most

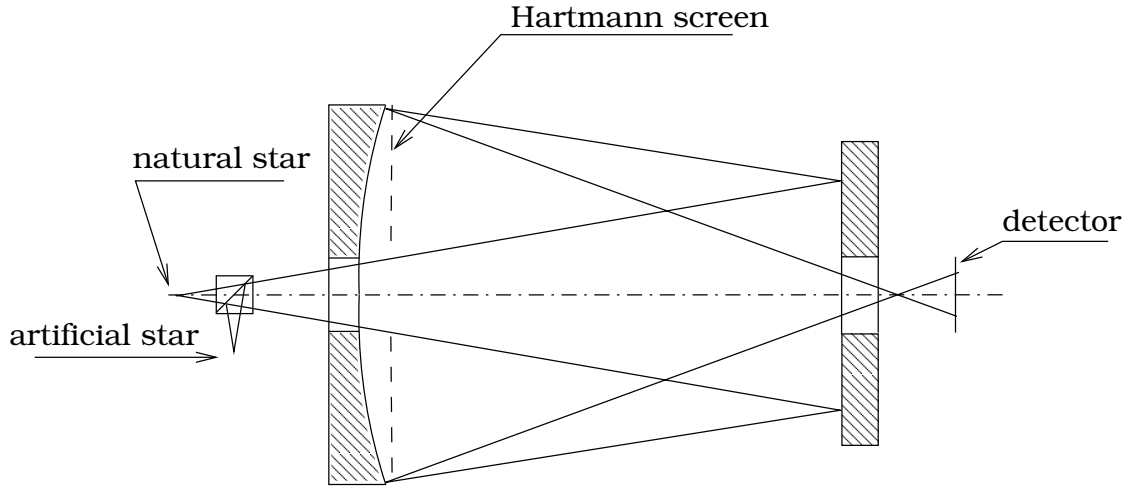
common method used for testing large mirrors during manufacturing is laser interferometry. This testing method is very sensitive to the disturbances caused by the air turbulence and mechanical vibration. Due to vibration sensitivity very short exposures must be used, which freezes the air turbulence effects. Several tens of measurements are usually averaged to obtain reliable results of the mirror shape. This method applied for the testing of mirrors of 8 m class required special arrangements such as huge vacuum chambers and special arrangement for vibration isolation due to the long light path the large air volume needed for testing these mirror.

The Hartmann testing method is insensitive to the turbulence and the vibrations, because it is possible to use long exposures to smooth out these effects. However, very modest sampling is possible, and in testing large mirrors photographic detection must be used due to the large size of the test image. This leads to a time consuming measuring process and analysis.

The Korhonen-Hartmann test is an interferometric modification of the Hartmann test. Also with this test, the turbulence and vibration effect can be eliminated by using long exposure time. In this modification, the detection occurs very close to the focus, resulting in a much reduced image size. The detection can therefore be performed with a CCD. Also much better sampling is possible.

A flat mirror and an elliptical mirror are used to re-image a star in front of a CCD camera. A mask (Hartmann screen) consisting of an array of holes, mounted near the elliptical mirror allows the sampling of the pupil (see figure 2.1).

Figure 2.1: Korhonen-Hartmann wavefront sensor.



In This plane, one can observe the Fourier transform of the screen, a grid of airy spots that can be write under the form:

$$I(x, y) \propto \left| \text{II} \left(\frac{Dx}{\lambda f}; \frac{Dy}{\lambda f} \right) \cdot \lambda f \frac{J_1 \left(\frac{ar}{\lambda f} \right)}{r} \otimes PSF \left(\frac{x}{\lambda f}; \frac{y}{\lambda f} \right) \right|^2 \quad (2.1)$$

where D is the distance between the holes, f the distance between the mask and the focal plane (figure 2.2), and $r = \sqrt{x^2 + y^2}$. When defocusing, the corresponding amplitude $U(x, y)$ evolve to give at a distance d :

$$U_d(x, y) = U(x, y) \otimes h(r) \quad (2.2)$$

where $h(r)$, the point spread function of the free space is:

$$h(r) = -\frac{i}{\lambda d} e^{ikd} e^{i\pi \frac{r^2}{\lambda d}} \quad (2.3)$$

At a reasonable distance one obtained a figure similar to the screen, where the spot are about the same size as in the focus, but with strong primary maxima, and weak secondary maxima. In the stellar images, the position of the spots is slightly, different than in the calibration image because of the wavefront error. One can obtain profiles of the wavefront parallel to the coordinate axis X and Y with a step-by-step integration (T Korhonen software) or with a least squares fit (M. Andersen software) using equations 2.4 and 2.5. Then the profiles are combined, and a least squares fit with the best fitting reference sphere is made. A good distance between the detector and the focus is $d = \lambda \left(\frac{f}{D}\right)^2$, and a ratio of hole separation to diameter between 2:1 and 3:1 has proven to give good interferograms.

Basically, one can consider that each square group of 4 holes produces one spot. Let us call X_A and Y_A the error in position of the spot given by a perturbed wavefront through a set of 4 holes in regard to the reference position given by a perfectly spherical wavefront, in the detector plane. Then if $\delta_1, \delta_2, \delta_3$, and δ_4 are the local wavefront errors for the holes 1,2,3, and 4 (figure 2.2), one can write:

$$\delta_3 - \delta_2 = \frac{\sqrt{2}DX_A}{f} \quad (2.4)$$

$$\delta_4 - \delta_1 = \frac{\sqrt{2}DY_A}{f} \quad (2.5)$$

With the calibration light source the spots are very sharp, and the measurement of their position is very accurate. In the stellar image, the spots are broadened due to atmospheric turbulence, and the accuracy of the measurements vary with the seeing condition.(see figure 2.3).

Computing the difference of position of the spots between the stellar image and the reference image, one can then calculate the shape of the wavefront.

2.1.2 Build-in wavefront sensor

The build-in wavefront sensor, which design is represented in figure 2.1, is also equipped with a removable lens in between the two mirrors. The use of this lens is to re-image the focal plane of the telescope on the CCD, in order to focus the telescope, and to make certain that the natural star is being centered on the position

Figure 2.2: Korhonen-Hartmann wavefront sensor principle

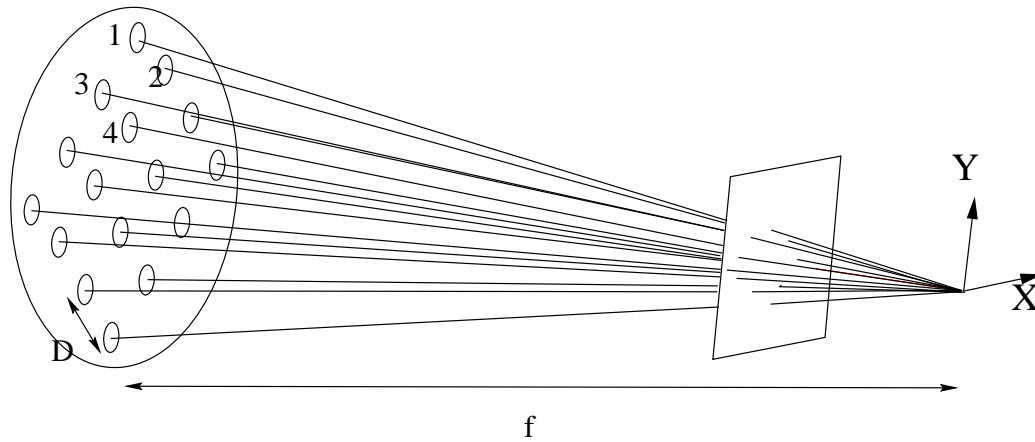
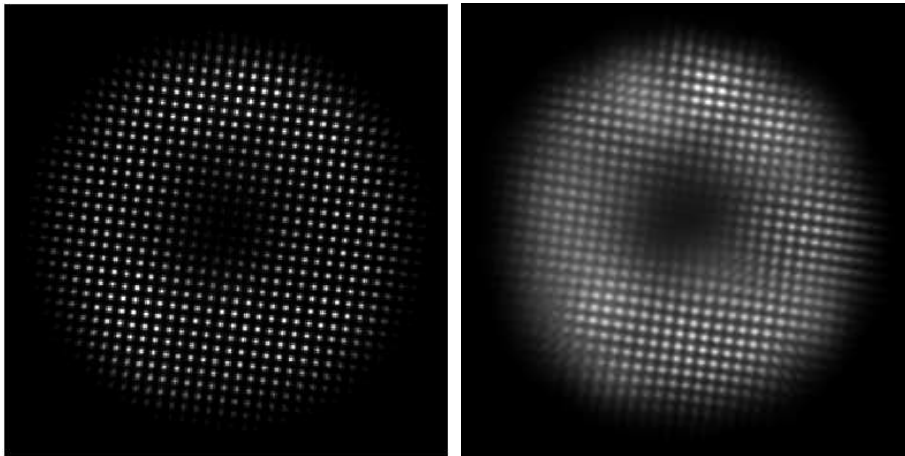


Figure 2.3: Calibration and stellar images with K-H wavefront sensor.



of the calibration star. Due to the misalignment of the wave front sensor, resulting in time consuming acquisition of the star, and camera control and reduction software, which is not so easy to use, the build-in wavefront sensor had not been used often. I realigned it (see Appendix A), and found that the mechanic isn't adapted to a moving device such as a telescope. Indeed, after having finished the alignment in the sea level office , and having mounted the wavefront sensor on the telescope, the alignment appeared to be completely wrong again. The screws which were holding the mirrors had gotten loose in the journey or in the handling. After aligning it again, I found that the focused star was not at the same place that it was on the table. It appeared that because of a difference in orientation, the weight of the arm holding the lens affects the position of the star. This is a minor problem, since it is unrelated to the images used for computing the wavefront. However, there is a more critical problem: the calibration star seems to be unstable, and one can see

some strong variations in the illuminance distribution of the calibration.

2.2 Curvature sensing

The curvature sensing method, developed by C. Roddier [3], works by making the difference between two defocused images, one pre-focal, and one post-focal. The defects of the wavefront implies small variations of the curvatures, and as a result, an excess of illumination on one image, and a lack of illumination on the other (see figure 2.4).

Figure 2.4: principle of curvature sensing

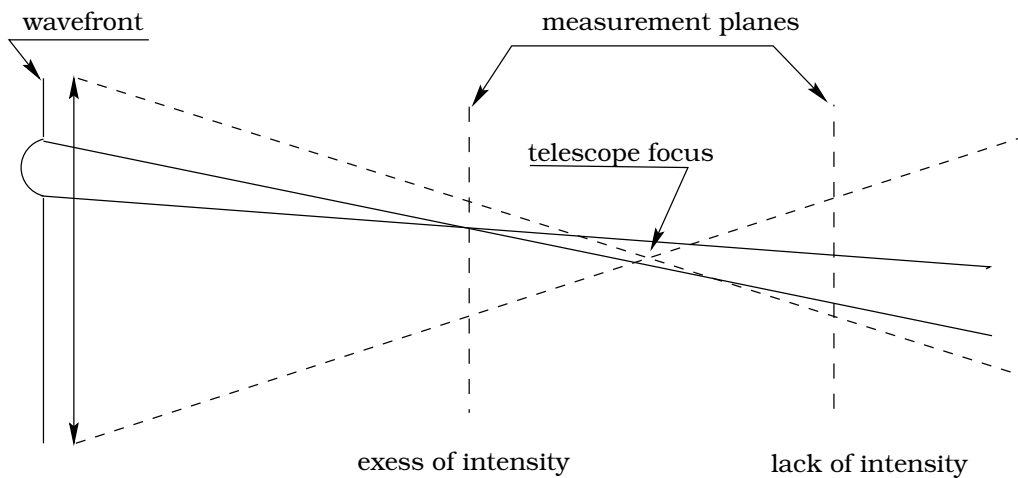


Figure 2.5 shows 2 extra focal images. One can clearly see on the polishing rings that what appears bright on one image appears dark on the other. By measuring the difference of intensity between the two images one can compute the wavefront figure. The theory is best described in terms of the irradiance transport equation. Assuming a paraxial beam propagating along the z axis, the irradiance transport equation states that:

$$\frac{\partial I}{\partial z} = -(\nabla I \cdot \nabla W + I \nabla^2 W) \quad (2.6)$$

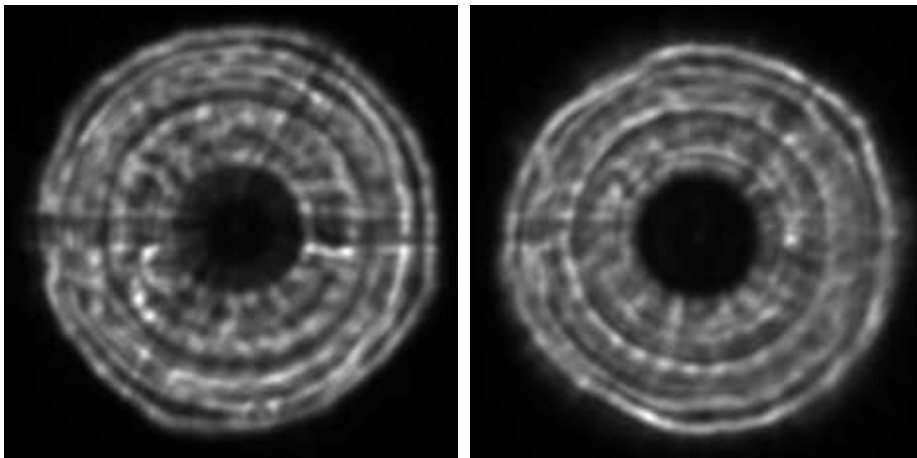
This equation is applied to the pupil plane ($z=0$) where the illumination is assumed to be fairly uniform and equal to I_0 inside the pupil and 0 outside. In this plane $\nabla I = 0$ everywhere but at the pupil edge, where

$$\nabla I = -I_0 \hat{n} \delta_e \quad (2.7)$$

δ_e is a linear Dirac distribution around the pupil edge and \hat{n} is a unit vector perpendicular to the edge and pointing outward. Putting Eq.2.7 into Eq.2.6 yields

$$\frac{\partial I}{\partial z} = I_0 \frac{\partial W}{\partial n} \delta_e - I_0 P \nabla^2 W \quad (2.8)$$

Figure 2.5: Post-focal and pre-focal images for curvature sensing.



where $\frac{\partial W}{\partial n} = \hat{n} \cdot \nabla W$ is the wavefront derivative in the outward direction perpendicular to the pupil edge. $P(x,y)$ is a function equal to 1 inside the pupil and 0 outside. At the near field, or geometrical optics, one can approximate the illumination I_1 (before focus) and I_2 (after focus) by

$$I_1 = I_0 - \frac{\partial I}{\partial z} \Delta z \quad (2.9)$$

$$I_2 = I_0 + \frac{\partial I}{\partial z} \Delta z \quad (2.10)$$

from which the following quantity S is computed:

$$S = \frac{I_1 - I_2}{I_1 + I_2} = \frac{1}{I_0} \frac{\partial I}{\partial z} \Delta z \quad (2.11)$$

It should be noted that, since in practice images are recorded in the image space, one has to invert (rotate by 180 deg) one of the out of focus images before computing S . Putting Eq.2.8 into Eq.2.11 gives

$$S = \left(\frac{\partial W}{\partial n} \delta_e - P \nabla^2 W \right) \Delta z \quad (2.12)$$

The telescope objective re-image the beam cross section that is beyond the pupil plane at a distance l before the focal plane. According to Newton's law,

$$(\Delta z + f)l = f^2 \quad (2.13)$$

Hence

$$\Delta z = \frac{f(f+l)}{l} \quad (2.14)$$

putting Eq. 2.14 into Eq. 2.12 yields

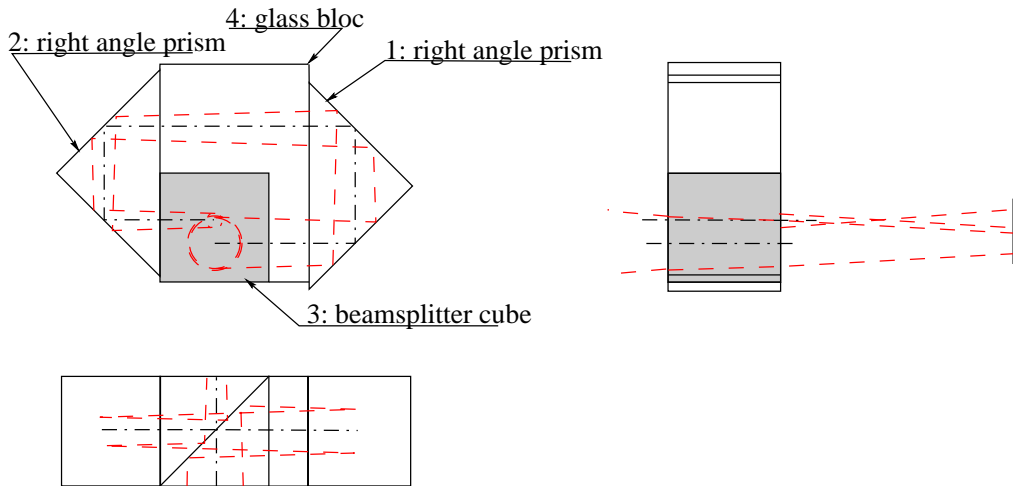
$$S = \frac{f(f+l)}{l} \left(\frac{\partial W}{\partial n} \delta_e - P \nabla^2 W \right). \quad (2.15)$$

This last equation shows that the sensor signal consist of two terms. The first term is proportional to the wavefront radial slope at the pupil edge and is localized at the beam edge. The second term maps the wavefront Laplacian across the beam. Since these two terms do not overlap, one can measure them separately and reconstruct the wavefront surface by solving a Poisson equation, using the wavefront derivative normal to the edge as a Neumann-type boundary condition.

The curvature sensing method is more accurate than the Hartmann method. Indeed, with this method the number of points of measurement is much higher than with the Hartmann method. In order to decrease the exposure time, it is useful to acquire both images at the same time. This can be done by focusing the telescope behind the CCD, splitting the beam, and retarding one the of the resulting beams on a lateral path so that it reaches focus before the CCD.

To be of practical use, the prism had to be accommodated in a filter holder for the standby camera. This would make it permanently available while still allowing the observer to use the standby camera for astronomical observations. I designed a prism which implements this function. This prism is made from a beam splitter cube, two right angle prisms, and a piece of glass in between. With this prism, one can obtain two beams with a defocus of 66mm, and a spatial separation in a plan perpendicular to the optical axis of 4mm. This separation can be adjusted by moving the right angle prism number one (see figure 2.6). Appendix D gives more information about the optical design of this prism.

Figure 2.6: Beam splitter prism for curvature sensing



Chapter 3

Results

3.1 Wavefront sensing to active optics relation

After having checked the state of the telescope, and before trying to implement any closed loop correction, it is necessary to know exactly how the active optics of the telescope works, what the real response of the telescope for one input active optics command is, and so on.

3.1.1 Active optics of the NOT

The axial support system of the primary mirror consists of 3 load cells and 45 bellows. The load cells act as zero force reference points and should ensure that the mirror is always kept at the same level independent of altitude. The 45 bellows, divided in 3 sections, apply local pneumatic forces on the mirror and therefore control the shape of the mirror.

6 different aberrations can be controlled by the the telescope control software:

- defocus
- coma
- spherical aberration
- astigmatism
- triangular coma
- Quadratic astigmatism

The focus and the coma are not controlled by the shape of M1, but by the position of M2. for each of these terms, one can set an amplitude of the deformation applied to the mirror (between $-2\mu m$ and $2\mu m$, peak amplitude) and an angle (between 0 and 360 degs). Because of some symmetry, in this representation the use of the angle is not always useful, and can be replace by only a negative amplitude. For example:

- the spherical aberration having a circular symmetry is not affected by the angle

- for the astigmatism, using opposite value of the amplitude is the same as adding ± 90 degs
- for the triangular coma, the same effect is noted for an adding angle of ± 60 degs
- for the quadratic astigmatism, one can use the opposite amplitude in spite of an angle of ± 45 degs

The active optics, currently works with some default values which gives the best image possible at zenith. This are recalculated after each aluminization, and some other time during technical period. The current ones are. :

| item | amplitude | angle |
|-----------------------|-----------|-------|
| focus | 0 | 0 |
| coma | 0 | 0 |
| spherical | -0.5 | 0 |
| astigmatism | 0.2 | 0 |
| triangular coma | 0 | 0 |
| quadratic astigmatism | 0 | 0 |

We first measured the output wavefront for the default values. For each of the aberrations, we then increased the amplitude by 1μ , took a measurement, and then again took another measurement after having decreased the amplitude of this same aberration by 1μ . The measurements were concluded by a new measurement with the default settings, to check if any drift had occurred while the measurements were acquired. This gives us a way of knowing the coefficient between the input value and the output wavefront error, and the modes of the mirror exited by each term. Doing the same measurements with all the 3 wavefront sensors, one can also compare the two methods, and the 3 devices.

3.1.2 Active optics to curvature sensing relation

The curvature sensing software (*ef* by Laplacian Optics) outputs the result of a reduction as a list of Zernike coefficients given in RMS nm. They can be easily convert in peak normalisation by multiplying by $\sqrt{n+1}$ when $m=0$ and $\sqrt{2} * (n+1)$ when $m \neq 0$. All the non circular symmetric aberrations are given with two Zernikes coefficient (one for the sinus part, and one for the cosines part). Let us call A_c the cosines coefficient, A_s the sinus coefficient, A and θ the amplitude and the angle in the active optics notation. Then one have the relations:

$$\theta = \arctan\left(\frac{-A_s}{A_c}\right) \quad (3.1)$$

$$A = \frac{-A_s}{\sin\theta} = \frac{A_c}{\cos\theta} \quad (3.2)$$

Each measurement has been made on a set of 6 images (3 pre-focal, and 3 post-focal). Calculating the Zernikes for each combination of one pre focal image, and one post focal image, one can evaluate the noise affecting the measurements. The Zernike coefficient has been calculated as far as the 22^{nd} (spherical 6^{th} order) which is the default configuration of the software. We then know a bit more about the higher order Zernikes without slowing down significantly the reduction. figures 3.1 to 3.4 are the results of this investigation. For each calculated aberration one have two graphs, one for the amplitude, and one for the angle. The Y axis gives the amplitude (or the angle), while on the X axis is plotted which aberration has been changed in the control system(default 1^{st} measurement, coma $+1\mu$, coma -1μ ,spherical $+1\mu$, spherical -1μ ,astigmatism $+1\mu$, astigmatism -1μ ,tri. coma $+1\mu$, tri. coma -1μ ,quad. astigmatism $+1\mu$, quad. astigmatism -1μ , default 2^{nd} measurement).

Figure 3.1:

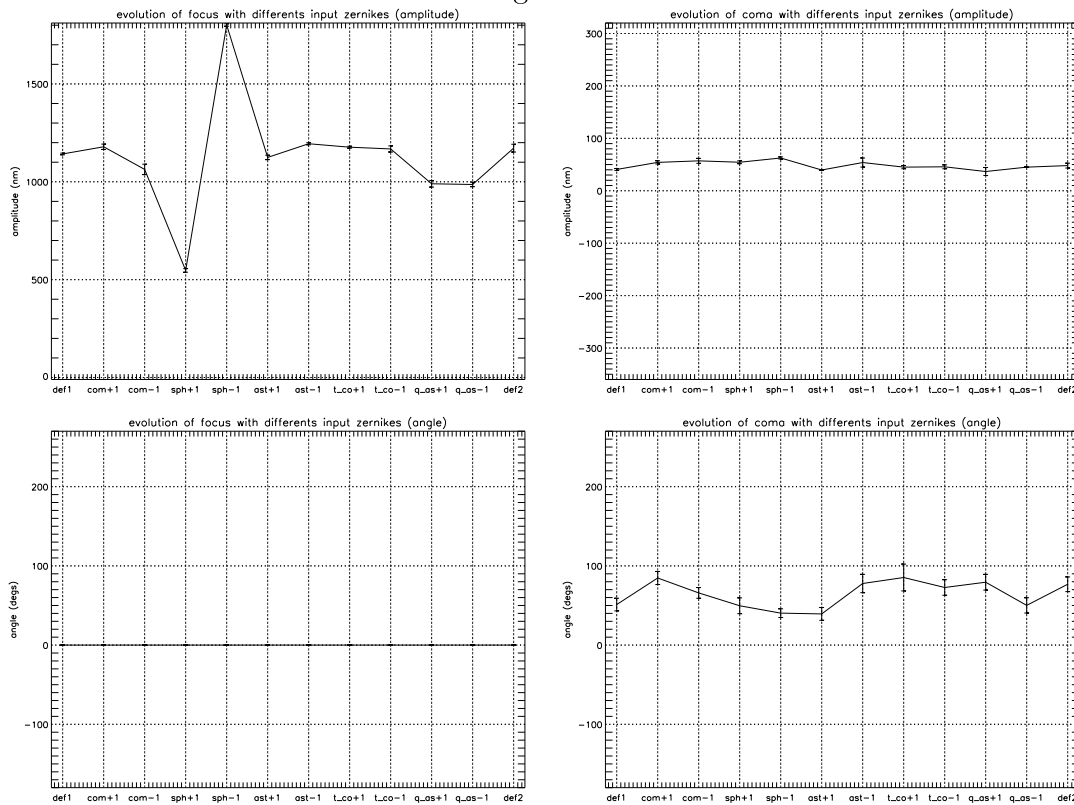


Figure 3.2:

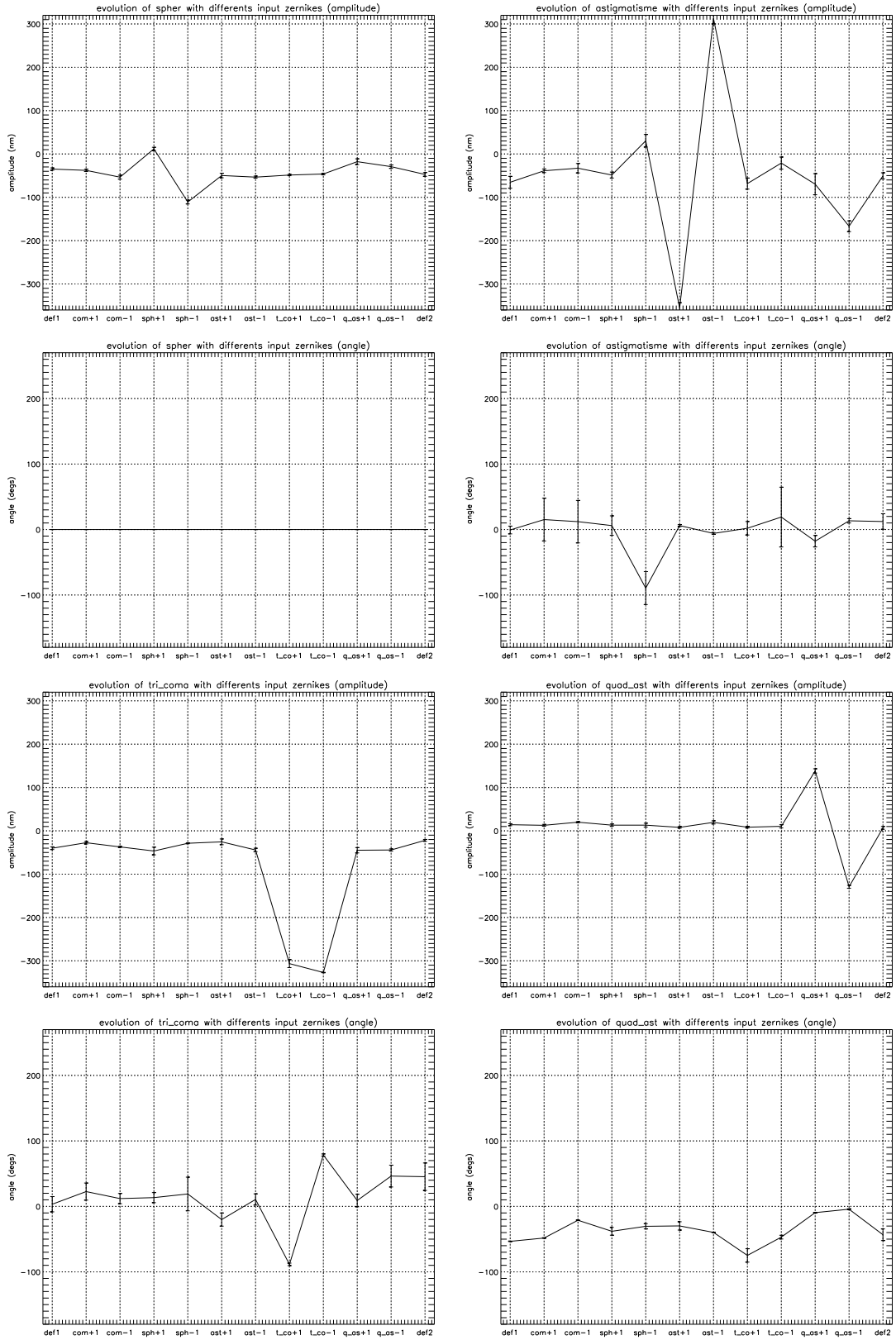


Figure 3.3:

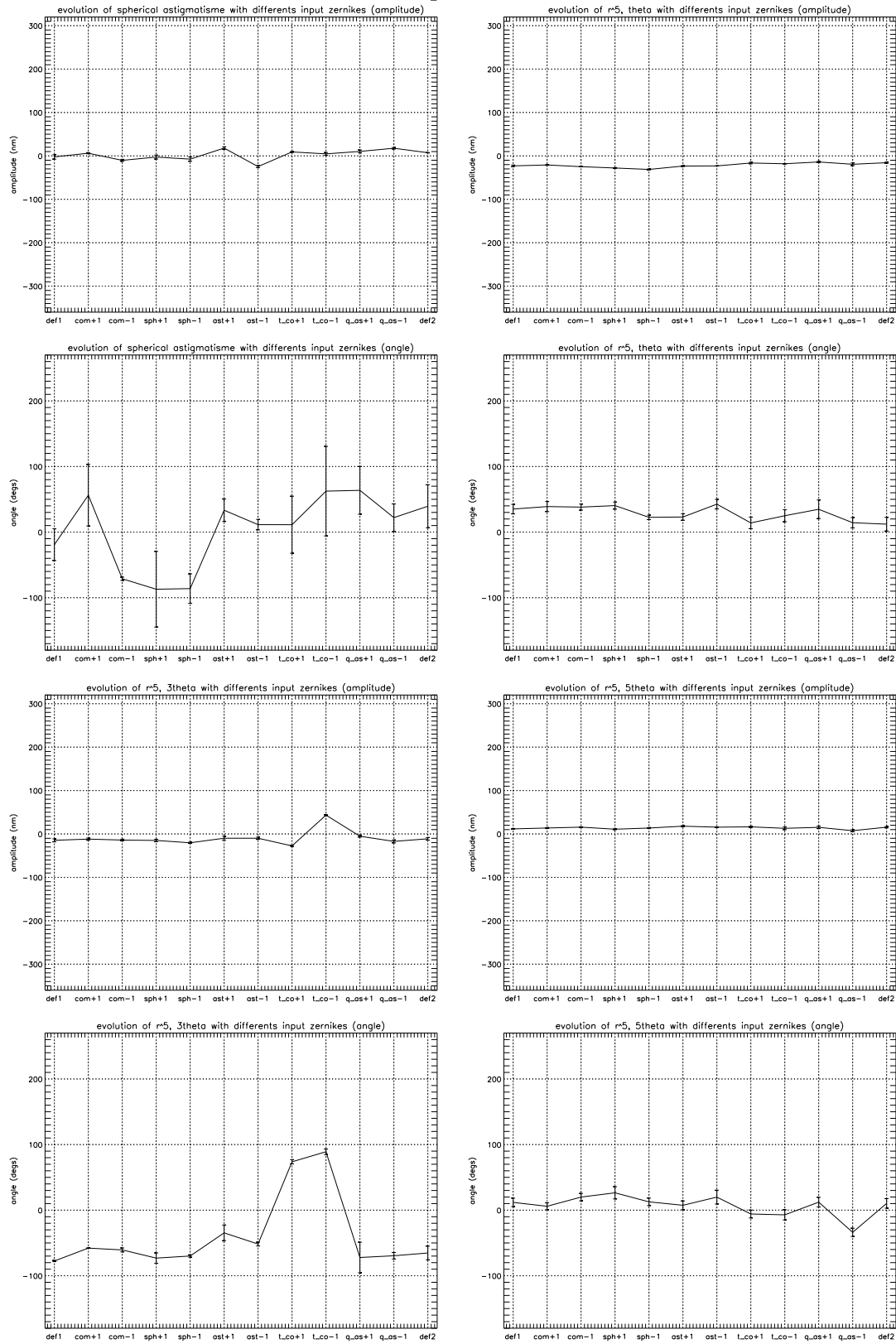
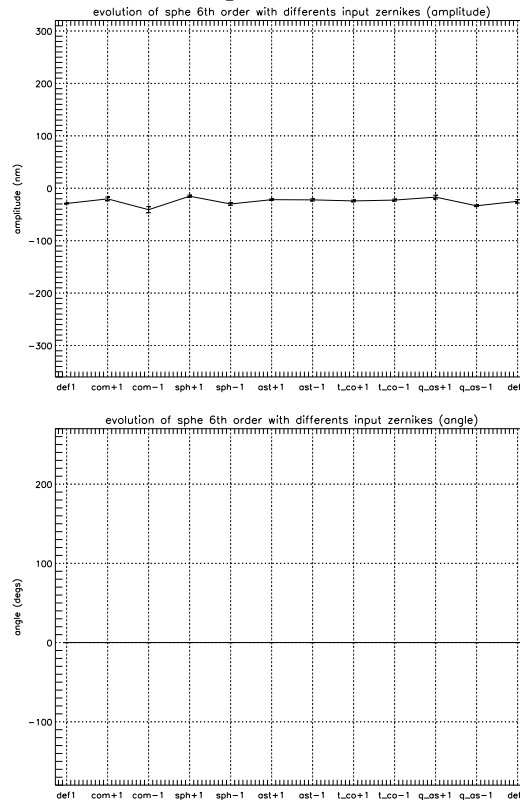


Figure 3.4:



One can clearly see from these graphs the response of the active optics for each input. All the aberrations are excited as they should be, except coma. This can also be seen by direct observation of defocused stars on the guide probe TV in the control room. All the terms give very particular figures to the image, but the coma. It is then clear that the implementation of the coma in the active optics doesn't work. It may have been the intention that coma correction should be done by using the two tilt movements of M2, but that the implementation of this was never completed. One can also see that the focus of the telescope is strongly influenced by the spherical aberration. This item of the active optics affect even more the focus than the spherical aberration. In fact, this aberration is of sufficiently high order that it is difficult to correct with only three rings of actuators. It is therefor not surprising that the result is a lot of focus (spherical aberration contains focus) and little spherical.

with these measurements, one can easily calculate the active optics to curvature sensing coefficients. Table 3.5 shows the results of this calculation. Horizontally are the excited Zernikes, and vertically the input item (the coefficients are in RMS nm/Peak μm , and then give the direct relation between the TCS input and the curvature sensing output). Since the coma doesn't work, I didn't include the corresponding input item in the table.

Figure 3.5: active optics to curvature sensing coefficients(nm/ μm)

| | focus | coma | spher. | ast. | t.coma | q. ast. | s. ast. | $r^5 \cos\theta$ | $r^5 \cos3\theta$ | $r^5 \cos5\theta$ | spher. 6 th ord. |
|----------|-------|------|--------|------|--------|---------|---------|------------------|-------------------|-------------------|-----------------------------|
| spher | 630 | | 60 | | | | | | | | 7 |
| astig | | | | -330 | | | 20 | | | | |
| tr. coma | | | | | -313 | | | | | | |
| qu.ast. | | | | | | 132 | | | | | 8 |

For more consistency we can convert these coefficient in peak input amplitude to peak output aberration. Table 3.6 gives these converted coefficients in μ/μ :

Figure 3.6: active optics to curvature sensing coefficients (with peak normalisation)

| | focus | coma | spher. | ast. | t.coma | q. ast. | s. ast. | $r^5 \cos\theta$ | $r^5 \cos3\theta$ | $r^5 \cos5\theta$ | spher. 6 th ord. |
|----------|-------|------|--------|-------|--------|---------|---------|------------------|-------------------|-------------------|-----------------------------|
| spher | 1.09 | | 0.13 | | | | | | | | 0.02 |
| astig | | | | -0.81 | | | 0.06 | | | | |
| tr. coma | | | | | -0.88 | | | | | | |
| qu.ast. | | | | | | 0.42 | | | | | 0.2 |

The most unexpected result of these measurements, is that the coefficient between the active optics and the calculated Zernikes is not the same for each aberration. The small coefficients for spherical aberration and quadratic astigmatism can be explain by the fact that these two are already high order aberration Then it becomes difficult to correct them with only three rings of actuators. One can notice also, a few "secondary" modes exited by the input one. This is the case of the spherical astigmatism exited by the astigmatism, for " $(r^5;3\theta)$ " exited by the triangular coma, and for the 6th order spherical aberration exited by both spherical and quadratic astigmatism. All the secondary modes exited are of the same nature as the input item, but the spherical 6th order (in regard to the Quadratic astigmatism) for which one can notice that it is so small, that it could also be normal noise from seeing variation. These "secondary" effects are very small (around 10 times fainter, than the principal one), and can easily be forgotten. On the variation of " $(r^5;3\theta)$ " term by triangular coma, on the behaviour of the angle is also sometimes quite strange. One can see some significant variations of angles on the evolution of astigmatism, triangular coma, spherical astigmatism, and " $(r^5;3\theta)$ " term. For the triangular coma, everything is normal. The drop of 90 degrees when one applies $1\mu\text{m}$ of amplitude, simply reveals that the 0 angle axis of the active optics is different than the one of the images (we took them with rotator position = -90 degrees). Then the 180 degrees difference given for the measurement with $-1\mu\text{m}$ is completely in agreement with the geometry of this aberration. Indeed its value oscillate with a period of 120 degrees, and then adding 60 degrees (modulo 120) to the angle invert the amplitude. For the astigmatism, and the spherical astigmatism, one can see

some change of the angle for input aberration which shouldn't have any effect. The explanation can be found by observing the amplitude when this variation occurs. Each times, the amplitude is near 0 nm, the angle becomes ill-defined, and goes at random directions. For the " $(r^5;3\theta)$ " term, one can observe the same effect as for the triangular coma.

3.1.3 The ALFOSC Korhonen-Hartmann WFS

The ALFOSC Korhonen-Hartmann WFS works after the principle described in sec. 2.1, except that it has all-dioptic optics. ALFOSC is a combined focal reducer and spectrograph. It is the most used instrument at the NOT. The optics is a dioptic system, having a collimated beam space with a pupil image. Two remotely controlled wheels allow for easy change for filters and grisms in this beam space. The ALFOSC WFS is placed in the grism wheel, which allows to position it at the location of the pupil image. This WFS consists of a mask and a singlet lens which changes the effective focal length of the ALFOSC camera. This makes it possible to obtain the focus offset, such that the interference spots are formed at the position of the detector. In front of the collimator, at the position of it's focus, is a slit wheel. In this wheel, a diode with a pinhole can be mounted. This acts as a calibration source for the WFS. When the WFS is used, a red filter centered at 650nm, is inserted in front of the WFS, in order to obtain the interference spots. The mask used produces useful 472 spots. Another wavefront sensor based on the same principle, which produces around 11000 spots is also available. Time did unfortunately not permit the use of this device.

3.1.4 Reduction of ALFOSC WFS measurements

The ALFOSC WFS images are reduced by IDL software, written by my supervisor M. Andersen. The procedure used is linear least squares fit of Zernike polynomials to the wavefront slopes. This software also allows to make simulated interferograms with a set of aberrations specified, including photon and detector noise. In this way it is possible to verify the reduction procedure. From simulations, it is found that all aberrations, at least up to Z16, are estimated to within 10%, with the exception of spherical aberration, where some of the aberration is fitted as focus. This is not surprising, because the measurements do not cover the edge of the pupil very well. The simulations also show that the WFS produces 'orthogonal results', i.e. if only one Zernike term is input, only one is output. When fitting real measurements, the typical error between the spot position and the fit corresponds to 15nm wavefront slope error, when fitting 22 Zernike terms.

3.1.5 Active optics to ALFOSC WFS relation

The same series of measurements which was done with the curvature sensing for mapping the behavior of the active optics, was also done with ALFOSC. For each setting, three measurements were made, such that the noise could be determined.

The results are in general quite similar to those obtained with the curvature sensing method. The relation between applied active optics settings and measured wavefronts is given in table 3.7, in μm peak aberration.

Figure 3.7: Active optics to ALFOSC wavefront sensor coefficients (with peak normalisation)

| | focus | coma | spher. | ast. | t.coma | q. ast. | s. ast. | $r^5 \cos\theta$ | $r^5 \cos 3\theta$ | $r^5 \cos 5\theta$ | spher. 6 th ord. |
|----------|-------|------|--------|-------|--------|---------|---------|------------------|--------------------|--------------------|-----------------------------|
| spher | 1.20 | | 0.17 | | | | | | | | |
| astig | | | | -0.77 | | | 0.07 | | | | |
| tr. coma | | | | | -0.77 | | | | 0.2 | | |
| qu.ast. | | | | | | -0.70 | | | | | |

The amplitude of spherical, astigmatism and triangular coma agrees very well with the curvature sensing results. A quite significant $r^5 \cos 3$ term is found for the triangular coma. This was not noticed in the curvature sensing result. The only major difference is that quadratic astigmatism is found to have the opposite sign and a significantly higher amplitude. The sign error can be explained wither by software or a mistake during observation. The difference in amplitude is more difficult to understand. The measurements obtained with the ALFOSC wavefront sensor appears to be less noisy than the curvature sensing results. As the data were taken on different nights, this difference may have been caused by different seeing conditions.

3.1.6 Active optics to build-in WFS relation

For the build-in wavefront sensor, the same series of measurements as with curvature sensing and the ALFOSC WFS, was obtained. In general it was found that the RMS noise of the fits was around 30nm, when fitting 21 terms. This is twice as much as found with the ALFOSC wavefront sensor. The difference is most likely due to a somewhat poorer detector and the fact that no filter is used with this sensor. As shown in table 3.8, the results are however very similar to those obtained with the other methods.

Figure 3.8: active optics to build-in wavefront sensor coefficients (with peak normalisation)

| | focus | coma | spher. | ast. | t.coma | q. ast. | s. ast. | $r^5 \cos\theta$ | $r^5 \cos 3\theta$ | $r^5 \cos 5\theta$ | spher. 6 th ord. |
|----------|-------|------|--------|-------|--------|---------|---------|------------------|--------------------|--------------------|-----------------------------|
| spher | 1.01 | | 0.13 | | | | | | | | |
| astig | | | | -0.85 | | | 0.09 | | | | |
| tr. coma | | | | | -0.81 | | | | 0.13 | | |
| qu.ast. | | | | | | -0.66 | | | | | |

For the build-in wavefront sensor, the derived amplitudes are all within the range of those found with curvature sensing and the ALFOSC wavefront sensor. We can therefore conclude that the three methods deliver approximately identical results, with the differences being without importance for actual, maybe with the exception of quadratic astigmatism. Simulated Korhonen-Hartmann measurements give the correct amplitude to 5%, suggesting that the 35% smaller amplitude found by curvature sensing is related somehow to that method. One small detail to note is that the sign of quadratic astigmatism agrees with that of the curvature method, as opposed to the results with the ALFOSC wavefront sensor. The sign (error) of the quadratic astigmatism as obtained with the ALFOSC WFS may therefore be due to mess-up of signs during the observation.

3.2 Behavior of the telescope optical aberrations

Until now, there had been made no attempt to monitor the behavior of the telescope aberrations over longer periods. Hence it was in reality unknown how much the image quality changes from night to night. During August and the beginning of September, we attempted to record wavefront sensing images during as many nights as possible. Several problems caused that only the data from seven nights could be used. It is not much, but still it is the most complete set of data ever made at the NOT for testing the behavior of the telescope optics.

Figure 3.9: behavior of coma and spherical

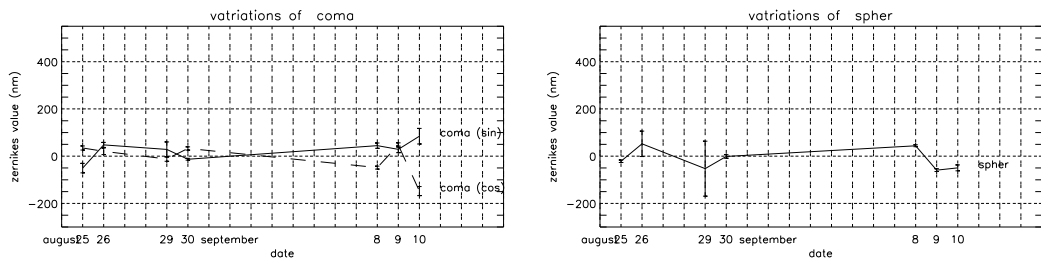


Figure 3.10: behavior of astigmatism and triangular coma

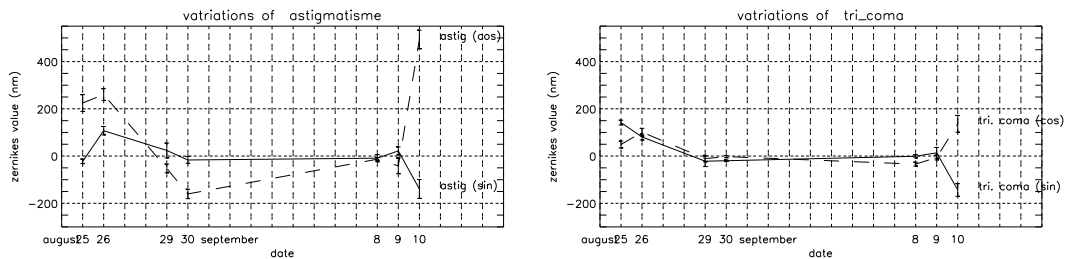
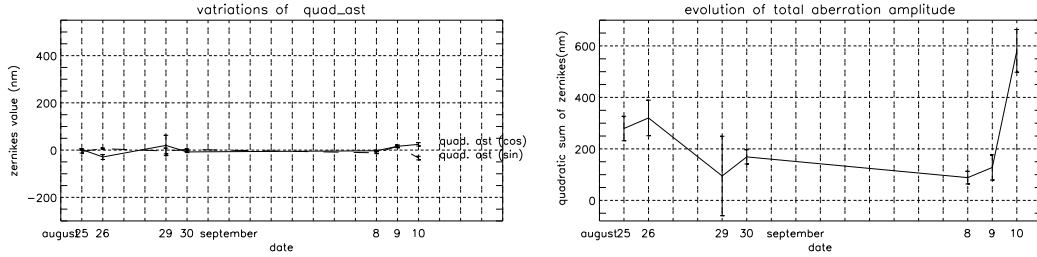


Figure 3.11: behavior of quadratic astigmatism and grand total amplitude Zernikes



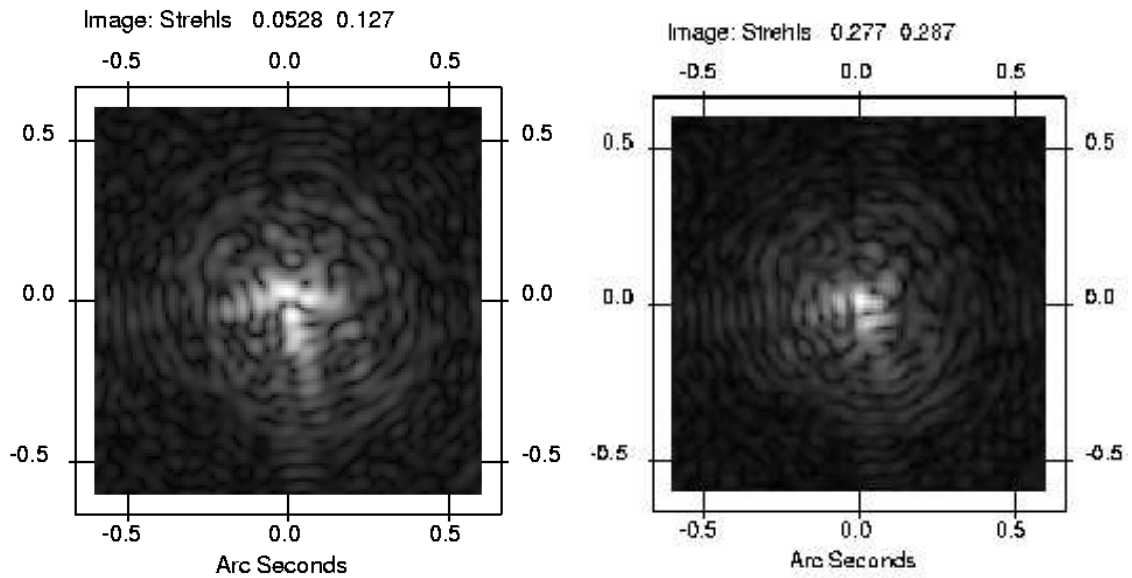
Figures 3.9 to 3.11 show the peak variation for the main aberrations. On these plots, I have subtracted the weighted average of the measurement (average where each measurement is weighted by the invert of its error), to show only the variations. All the measurement have been made at a low zenith distance (between 2 and 10 degrees) using *StanCam*, but the 10 September's one has been made with an other instrument (*HiRAC*). This is likely the reason for the inversion which can be observed for this date (the relative orientation of the CCD in *StanCam* and *HiRAC* might be different by 90 degrees, which invert the sine, and the cosine axis). All the aberrations but the quadratic astigmatism shows big variations which seems completely random, and astigmatism appears to be the most varying aberration. It is difficult to know which parameter influence these variations. It is possible that a part of it comes from the low zenith distance, where it is known that horizontally stratified temperature structures within the telescope center section and it's baffles may build up. As one will see in the altitude dependence study, the measurement at low zenith distance are more noisy than at higher zenith distance, and hence less reliable. Still, the variations seems to be too important to be only due to this, and then, one would need now other set of measurements to complete the analysis of the behavior. These news measurement should be taken around 45 degs altitude to avoid the effect of low zenith distance, and pointing the telescope towards the wind, to avoid the influence of local seeing. Such a measurement every night with good seeing and wind speed in the range 2-8m/sec would allow us to see if there is any continuous variation, or if each nights observation is uncorrelated with the precedent one. Also, it could be useful to record weather informations such as temperature, wind direction and speed, and humidity to see if these parameters correlate with the observed variations. The grand total amplitude variation (figure 3.11), obtained with a quadratic summation on all the Zernike which can be corrected par the active optics, shows variation of the amplitude of ≈ 176 nm RMS, but a the last measurement taken with *HiRAC* has a big contribution in this variation, and since we don't really know how coherent this measurement is with the other ones, we decided not to take it into account. Then, the RMS variation of aberration amplitude is only 98 nm. This mean that a closed loop wavefront sensing and correction is not necessary under average seeing conditions. However, without closed loop control, the telescope will not be able to exploit the best seeing conditions available above La Palma. The variance of the seeing induced phase variations over the pupil is:

$$\sigma_{\varphi}^2 = 1.03 \left(\frac{D}{r_0} \right)^{5/3} \quad (3.3)$$

where D is the diameter of the pupil, and r_0 the Fried parameter. For $0''.5$ seeing and $\lambda=550\text{nm}$, r_0 is 0.2 m, giving a RMS phase error of 730nm. The seeing of the free atmosphere is often (5% of the time) as good as $0''.25$, corresponding to an RMS phase error of 410nm, or comparable to that of the telescope aberrations. The best seeing recorded at the NOT is around $0''.35$. The difference between the free atmospheric seeing and the seeing recorded at the focal plane is partly explained by the telescope aberrations.

More vivid, are maybe the computed bi-dimensional PSF, obtained for each measurement. Figure 3.12 shows this PSF at 500 nm for the 30th of august, and the 8th of September. The ≈ 120 nm difference in peak amplitude aberration leads to a drop of ≈ 0.2 on the Strehl ratio. If the same PSF is calculated in the IR ($2\mu\text{m}$) and not in the visible, one still can see a drop of 0.1 on the Strehl ratio, which is still important.

Figure 3.12: PSF at 500 nm on august 30 and September 8 1999



3.3 Altitude dependence of the aberrations

If the mechanical structure supporting the primary mirror, works as it has been designed for, the mirror, even given that it is very thin, should not be deformed by the influence of its weight, when pointing the telescope to different altitudes. Accordingly, the aberrations should be completely independent of the zenith distance. If this is not the case, we know that the support system is not working in an optimum way. There are two solutions to this: either the problem with the support system

is identified or altitude dependent aberration corrections are applied to the active optics system (as has been foreseen in the telescope control system) . While the first solution is the preferred one, the later may be the most realistic solution. Figure 3.13 to 3.15 shows the altitude dependence of the main aberrations.

Figure 3.13:

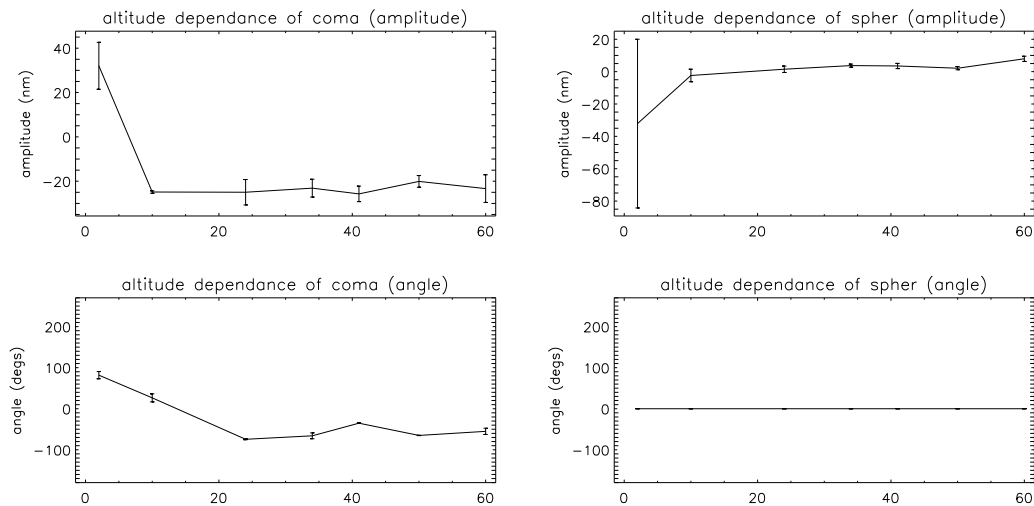
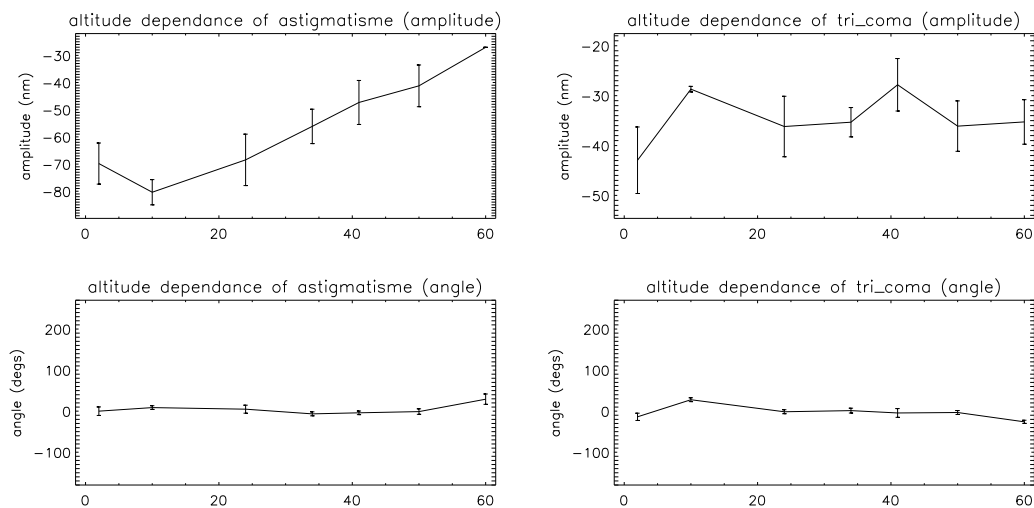


Figure 3.14:



As can be noticed, it is only for the astigmatism that a clear dependence with the altitude is evident. Most of the aberrations shows peculiar behaviour at low zenith distances. The values given for 2 degrees zenith distance should most probably not be taken into account in the study of the altitude dependence. These measurements are the most too noisy, as can be seen in figure 3.16,

Figure 3.15:

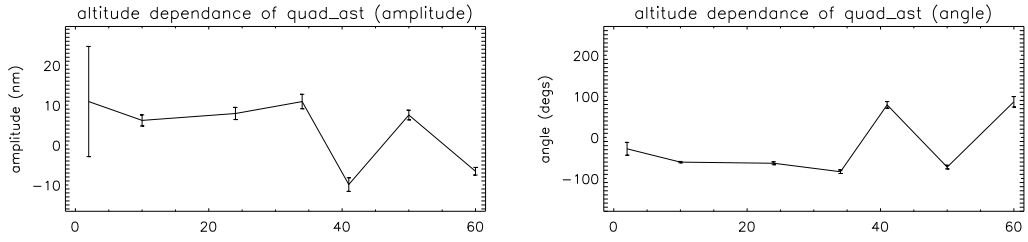
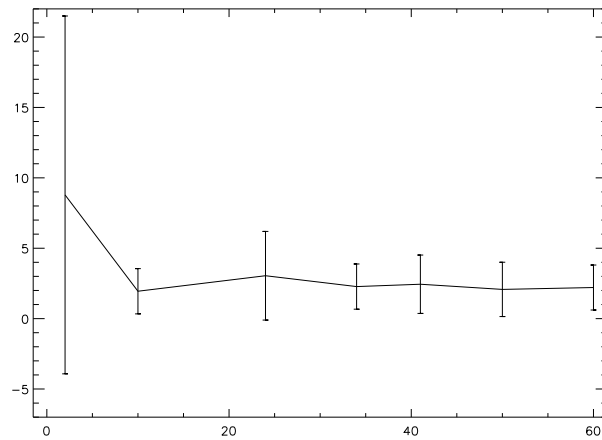


Figure 3.16: evolution of noise measurement with the pointing altitude



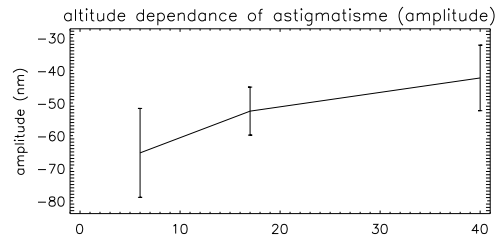
and it was even clear by looking directly at the images from this altitude that the results would not be reliable.

The apparently big variations which can be seen for the quadratic astigmatism for altitudes equal to 40 degs and 60 degs, are just coming from the fact that the angle is calculated between $\pi/2$ and $\pi/2$, and that the cosine part of this aberration (about 10 time smaller than the sinus part), is varying around 0 nm.

This set of measurements have been made without any filter in front of the CCD. My supervisor M. Andersen considered that atmospheric dispersion could affect the curvature measurement, giving rise to an apparent zenith dependence of notably astigmatism because of the elongated images. It should be noted here that the CCD's used are very sensitive at wavelengths from 350nm to 900nm, resulting in a dispersion of more than $2''$, corresponding to 10 CCD pixels or 7 % of the image diameter. We made a verification of this by taking a few more measurements at different altitudes, using a red filter in front of the CCD.

Figure 3.17 seems to show that the variation we observe for the astigmatism is also present in the measurements obtained with the red filter, but the measurement are quite noisy, and we can't be completely sure of this. Apparently, however the lateral supports of the primary mirror don't behave as they should, but the amplitude of

Figure 3.17: verification of altitude dependence of astigmatism



the evolution stays in the same limits than the day to day evolution, and a LUT would be of no use to correct this.

Conclusion

A big improvement in the knowledge of the telescope have been made with this project. We now know a lot more about how the active optics, and the telescope itself behave. The coma have never been implemented in the active optics system, and while the 'coma command' in this system is not connected to the top unit, one can't correct this term which contribute however for about one third in the image degradation. For the other aberrations, some coefficients have been found to establish a relationship between the TCS command, and the real aberration on the resulting wavefront. Spherical aberration and quadratic astigmatism are 4th order radial aberration, it is then difficult to correct them efficiently with only three rings of actuators. Finally then we can say that *only astigmatism and triangular coma can really be corrected by the active optics*

Everything possible have been made to get the M1 support optimized. Still, one can observe significant variations of the astigmatism with the observing altitude, and this reveals that something is wrong with this support system (design?? construction??) Since this variation is smaller than the one implied by the telescope behavior, one can't correct it with an altitude dependent look up table implemented in the TCS

With the study of the telescope behavior, we know now that the telescope itself adds about 10 % of variation to the seeing phase variation.

In spite of all this new knowledge on the telescope, one can say that this project has raised more questions than it has solved. Why are the lateral supports not fulfilling their requirements? Where do the night to night variations come from? There is then a lot of work to continue this project. More studies of the behavior must be done, recording in the same time some extra parameters in order to know what influences this behavior.

The curvature sensing seems the easiest way of measuring the wavefront. It can easily be automated, once a catalog of convenient stellar targets (≈ 10 magnitude), and the prism beam splitter made.

Bibliography

- [1] T.Korhonen,T.Lappalainen,A.sillanpää , "*Hartmann interferometric testing of large mirrors*", , Advanced Optical Manufacturing and Testing II, Larry D. Barr, Brian Macks, Editor, Proc. SPIE vol .1531, pp 44-49, 1991
- [2] T.Korhonen , "*interferometric method for optical testing and wavefront error sensing*", Advanced technology Optical Telescopes II, Larry D. Barr, Brian Macks, Editor, Proc. SPIE vol .444, pp 249-252, 1984
- [3] C.Roddier, F.Roddier "*wavefront reconstruction from defocused images and the testing of ground based optical telescopes*", J. Opt. soc. Am. A, Vol 10, No 11, pp 2277-2287, November 1993

Appendix A

Manual for aligning the telescope

The alignment of the telescope consist mainly in 4 different steps, 2 for each mirror: Centering and tilting. The reference for the alignment is the rotator axis, the mechanical axis around witch are the alignment is the rotator axis, the mechanical axis around which the instruments are turning

For the primary mirror (M1), these 2 steps require a special tool which can be mounted on the rotator axis. At the extremities, one can mount a LVDT, and a dial indicator (see drawing). The LVDT roll at the edge of the mirror and gives a measurement of the the tilt of the mirror (when the mirror is perpendicular to the rotator axis, the there is no displacement of the LVDT when the tool rotates). The dial indicator is mounted on the rim of the mirror and gives the lateral displacement of the mirror during the rotation, and hence the de-center of the mirror.

A.1 required tools

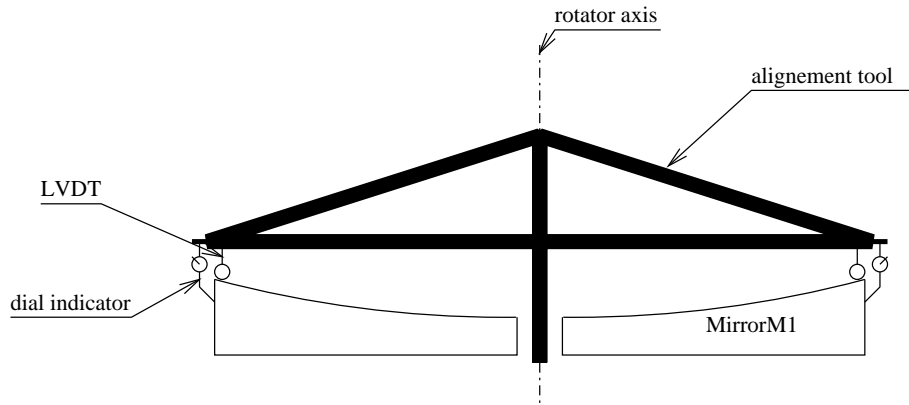
Several tools are required for aligning the telescope. Here is the list of these tools.

| | |
|------------------------------------|--|
| Long spirit level : | to measure the lateral support, and the planarity of M1 |
| Alignment tool: | for the alignment of the M1 (see drawing of the tool below) |
| Two dial indicators: | to measure the perpendicularity between the rotation axis and M1 |
| Two LVDT's with ball bearing head: | to center M1 with the rotation axis |
| Pupil imaging lenses for ALFOSC: | |
| Pupil imaging screen: | to align M2 |
| Black screen at rim of M2: | |
| Lamp: | for illumination of pupil imaging screen. |

IDL software for analyzing dial indicator/LVDT measurements.

IDL software for analyzing pupil images.

IDL software for calculating adjustments to spider.



A.2 Alignment at zenith.

A.2.1 Alignment of M1.

1. Installing alignment tool

First of all, one can install the alignment tool. To do this, you have to:

Disconnect M1 cover motors and baffle temp sensors, then take off center section rubber blocks, and get the internal stray light baffle out.
you can now remove M1 baffle, and mounting M1 alignment tool.

2. Centering of M1

Then one have to center M1 on the rotator axis. In fact, if the De-center is not big, it is easier to move the rotator and to center it on the mirror.

Mount dial indicators on cross bar, and mount dial indicators for M1-cell ref (2 dial indicators for X and Y position of the mirror mounting under the mirror with magnet holders)

The measurement itself: rotate cross bar 5 degs, check the indication of the dial indicator, do it again until you reach 180 degs, and analyze the measurements with M. Andersen analysing software .

Then, you have to correct the centering of M. To do this you have to loose the three lateral fixtures, shift M1 side vise in cell, tighten the three lateral fixtures, evacuate all bellows, and put M1 back on bellows.

Then, check that M1 is centered with the same method than above

3. Shimming of M1 cell.

Shimming M1 cell is the only way to ajust the tilt of M1. 4 points of shimming are used at the extremity of 2 orthogonal diameters of the mirror, one parallel with the altitude rotation axis, and the other one orthogonal with this axis. The followings steps are required to do it.

Dismount lateral supports 5,6,15,16 to have free access to the fixing point of M1-cell, and adjust load cells to M1 stress free position.

Measure alignment of M1.

- Mount LVDT's on cross bar, and Do measurements for each 5 degs (in the same way than for the centering), analyze the measurement with M Andersen software.
- Calcul thickness of shims.

Lower M1 cell one thread, add shims one by one, tighten M1-cell.

Mount lateral supports 5,6,15,16, and re-measure alignment of M1, then adjust the tilt using the active optics to obtain high accuracy alignment.

4. remove alignment tool.

Remove all measuring equipment, then glue rubber blocks back on center section.

Re-mount M1 baffle.

- Re-position M1 baffle support, put M1 baffle on its support, and re-mount it.
- M1 baffle support to obs floor.
- Put internal stray light baffle in.

Re-connect M1 baffle temp sensors. and re-connect M1 cover motors.

The following steps have been done during the summer 1999. They consist in putting the lateral support in the same plane as the mirror.

Measure altitude at which M1 is in level.

Measure orientation of lateral supports, for eac of them:

- make a horizontal reference level with a long aluminum bar, and calibrated thickness strips
- find the good gap between the support cells of the special tool to make it fit on the lateral support. (4 support cells of tiny different size are available, one small, two medium, and large, the list of the configuration which fits the best for each support is given in table A.1)¹.
- put the tool down on the aluminum bar, support cells laying on the horizontal reference, and measure the horizontality default of the tool.
- mount tool on lateral support, and measure the altitude at which the lateral support is horizontal (according to the horizontality default of the tool).

¹S=small cell, M=medium cell, L=large cell. The configuration is given from left to right when looking the tool with side which hold the spirit level

Table A.1: best tool configuration for each lateral support

| | | |
|----|---|---|
| 1 | M | L |
| 2 | M | L |
| 3 | M | M |
| 4 | M | L |
| 5 | S | M |
| 6 | P | L |
| 7 | M | M |
| 8 | M | L |
| 9 | M | L |
| 10 | L | S |
| 11 | M | L |
| 12 | M | L |
| 13 | S | L |
| 14 | M | L |
| 15 | M | L |
| 16 | S | M |
| 17 | M | L |
| 18 | M | M |
| 19 | L | S |
| 20 | L | S |

calculate the difference with M1 orientation.

Adjust LC's to lower M1, in order to get all lateral supports pointing down, and calculate thickness of shims which makes all support being in the plane of M1.

shimm lateral supports. For each support:

- loose the 6 screws which maintain the lateral support to the mirror, then remove all screws but the back one, while somebody is holding the counterweight
- add the shimm(s), putt back the screws, tighten them all

verify orientation of lateral supports

A.2.2 Alignment of M2.

Alignment of M2 is done by imaging the pupil on the detector of *ALFOSC* and observing the displacement of the image while rotating *ALFOSC*

Mount *ALFOSC* with pupil imaging lens, and mount flat field screen below spider, then set Tilt1,Tilt2 and disp. To 'neutral' pos.

Measure M2 position with pupil imaging lens. M2 is centered when its images through the pupil imaging lens doesn't move on the ccd. Center M2 by adjusting spider. Repeat this step until M2 is centered.

Dismount flat field screen, and measure exit pupil pos. with pupil lens: this is made by imaging M1 on ALFOSC CCD through M2 and the pupil imager. Here again the image must be stable when one rotate *ALFOSC* (MA,...). Then tilt M2 by adjusting spider, and repeat this until M2 aligned .

CO2 cleaning of M2.

A.2.3 Alignment on sky, pointing and active optics.

Check and adjust load cells on the sky, then update pointing model.

Re-set telescope parameter: update active optics constants, re-calibrate altitude dependence of focus, and re-calibrate displacement constant.

Check tilt of tel. focal plane with *ALFOSC* .

A.3 Alignment away from zenith. (to be done)

Measurements of optics position as func. of alt.

- Rotator axis tilt/displ with respect to M1.
- M2 tilt/displ with respect to M1.

Measurement of load cell reproducibility (new load cells??).

Full implementation of active alignment.

Appendix B

Manual for aligning the build-in wavefront sensor

This appendix is a manual for aligning the build-in wavefront sensor.

B.1 Required tools

- The external reference star (called ERS in the following sections): This tool, designed by V. Belmont and build by P. Brandt, consist of an aluminum tube screw on a circular plate which fits in the front side of the wavefront sensor. The tube contains a 40mm focal lens and an aperture stop. It is closed at one end by a pinhole, and at the other end by a disc with a hole drilled in the center to hold the light source (red LED)
- A red LED with a flattened front part
- CCD #2 and CCD controller
- Power supply.
- A sergeant to hold the ERS on the Wave-front sensor
- A set of Allen keys

B.2 Internal alignment

- focus internal calibration star on CCD by adjusting gap between the the 2 lenses which forms the focusing system.
- Focus ERS: just screw or unscrew the tube in the circular plate, until ERS is focused on the CCD.
- Center pinhole of ERS: when rotating the ERS (plate + tube), the focused images may not move on the CCD

- Align mirrors: the more difficult part, when taking long exposures, one might see a ghost circular image in addition to the spot image. The only way I found it possible to align the mirror is to co-center this ghost image, which is caused by direct light from the LED, and the spot image.
 - Center the mirror on the mechanical mount. One can check that the elliptical mirror is centered by rotating the ERS by 180 degs. The spots might not move.
 - adjust tilt of mirrors with the alignment screws on the back of each mirror to center the spot images on the ghost image. Adjusting alternatively one mirror and the other, this adjustment might converge.
- Centering of focused image of ERS: 2 adjustment screws are available on the arms of the removable focusing lens. By playing with these screws, one can center the focussed image on the spots image (note down the center of these image before taking a focused image, or better, add the focused images to the spots images, then one can easily see where the focused star is localized in regard to the spots one)
- Center pinhole of internal calibration star in order to get the maximum output intensity.
- Co-center internal calibration star with ERS: some adjustment screw are available on the beam splitter cube for this purpose.

B.3 Alignment with respect to the telescope

- Centering of wave-front sensor on rotator axis
 - Point to a bright star from catalog /catalog/wfs.cat, focus telescope. Center it on the rotator axis.
 - Move wave-front sensor until calibration star is confounded with natural star
 - engrave fixating point on fixating aluminum plate. Machine this plate (PB)
- center telescope pupil (must be done when *ALFOSC* is out)
 - Open mirror cover
 - Unmount CCD # 2
 - Move CCD probe to wavefront sensor
 - Observe telescope pupil trough wavefront sensor, and adjust tilt adjustment screws to make it center on the mask

Appendix C

Programming

In order to prepare an easy way of making Wavefront sensing, I wrote a batch program in tcl language (`auto_ef.tcl`) which run the curvature sensing software for a set of 3 post focal images, and 3 pre focal images automatically without using the graphical interface. the images must be in FIT format, without extension, and their name must finish with 4 numbers. The number of the pre focal images must follow themselves, as well as the numbers of the post focal images. An other (little) program written in IDL (`runef.pro`), runs `auto_ef.tcl` and returns the data (mean value, and error, for each aberration) ordered in the same way than in the TCL (focus, coma, spherical, astigmatism, trefoil, quadratic astigmatism, and then spherical astigmatism, . . . , spherical 6th order), and under the representation (amplitude, angle).

The following pages gives the source codes for these programs.

Program auto_ef.tcl

```
#begin{verbatim}

##### initialisation : no graphical output #####
set data_graphocity(display_on_load) 0
set data_graphocity(display_on_save) 0
set data_graphocity(display_mapped_images) 0
set data_graphocity(display_intermediate_wavefront) 0
set data_graphocity(display_final_wavefront) 0

ef_configuration_StanCam ##load telescope configuration for StanCam##
ef_setSequence_default

##### reading image directory and filename #####

set Id [open "donnee"]
gets $Id wd
if {$wd == ""} then {set wd .}
puts stdout "image directory is: $wd"

gets $Id fname1
puts stdout "first prefocal image is: $fname1"

gets $Id fname2
puts stdout "first postfocal image is: $fname2"

gets $Id zer
puts stdout "reduced data filename is: $zer.txt"

close $Id

##### computing filename of 2nd and 3rd image of each type ###

set size [string length $fname1]
set sepp [expr $size-4]
set sepm [expr $size-5]
set str11 [string range $fname1 0 $sepm]
set str12 [string range $fname1 $sepp e]

set cmpt 0
for {set i 0} {$i<2} {incr i} {
    if {[string range $str12 $i $i]==0} {incr cmpt}
}

```

```

append str11 [string range $str12 0 [expr $cmpt-1]]
set str12 [string range $str12 $cmpt e]

set size [string length $fname2]
set sepp [expr $size-4]
set sepm [expr $size-5]
set str21 [string range $fname2 0 $sepm]
set str22 [string range $fname2 $sepp e]
set cmpt 0
for {set i 0} {$i<2} {incr i} {
    if {[string range $str22 $i $i]==0} {incr cmpt}
}
append str21 [string range $str22 0 [expr $cmpt-1]]
set str22 [string range $str22 $cmpt e]

### reducing data ###

for {set i 0} {$i<3} {incr i} {
    for {set j 0} {$j<3} {incr j} {
        set f1 ""
        set f2 ""
        set s1 [expr $str12+$i]
        set s2 [expr $str22+$j]
        append f1 $str11 $s1
        append f2 $str21 $s2
        puts "calculate zernikes on files $f1 and $f2"
        ef_addFileCmdLine $wd $f1 1
        ef_addFileCmdLine $wd $f2 2
        ef_seq c1
        set prog_param(save_path) .
        puts "$prog_param(save_path)"
        ef_saveZernikesCmdLine c1 Noll 4 22 text $zer a+
    }
}
#end{verbatim}

```

Program runef.pro

```
function runef, sum

;+
; NAME:
;     runef
;
; PURPOSE:
;     run curvature sensing batch file auto_ef.tcl, order the data,
: and give them under the representation (amplitude, angle)
;
; CALLING SEQUENCE:
; data = extract_curv_data([sum])
;
; INPUTS:
;     none
;
; OUTPUTS:
; data = (2,2,11) dimension array with amplitude (data(0,0,*))
: and angle (data(0,1,*)) for the aberrations from focus
: to spherical 6th order, and their
; standard deviations ( data (1,*,*))
;
; OPTIONAL OUTPUTS:
; SUM contain the quadratic sum of zernikes and standar deviation
;
; COMMON BLOCKS
;     none
;
; SIDE EFFECTS
;     none
;
; RESTRICTIONS
;     Needs function extract_curv_data
; the extra focal images must have been take with StanCam,
: and StanCam telescope configuration must be recorded in used
; .ef_configuration.tcl file
;
; MODIFICATION HISTORY:
;     WRITTEN, BELMONT vincent, NOT, october 1999
;-

;***** initialisation *****
```

```

a= ''
s=strarr(4)

print,'enter image file directory: '
read,a
s(0)=a

print,'enter first prefocal image filename: '
read,a
s(1)=a

print,'enter first postfocal image filename: '
read,a
s(2)=a

print,'enter file name for saved reduced data (without extension): '
read,a
s(3)=a

openw,1,'donnee'
for i=0,3 do printf,1,s(i)
close,1

;***** data reduction *****

print,'wait while data reduction is running...'
spawn,'ef -batch -e auto_ef.tcl'

;***** data formatting *****

data=extract_curv_data(s(3)+'txt',sum)

return,data
end

```

Programm extract_curv_data.pro

```
;+
; NAME:
;     extract_curv_data
;
; PURPOSE:
;     extract zernikes from "EF" software output textfile, class data in same
;     than active optics items, and put aberrations under the form (amplitude,
;     angle)
;
; CALLING SEQUENCE:
; data = extract_curv_data(file, sum )
;
; INPUTS:
;     file = zernikes text files from EF
;
; OUTPUTS:
; data = (2,2,11) dimension array with amplitude and angle for the
; aberrations from focus to spherical 6th order, and their
; standard deviations
;
; OPTIONAL OUTPUTS:
; SUM  contain the quadratic sum of zernikes and standar deviation
;
; COMMON BLOCKS
;     none
;
; SIDE EFFECTS
;     none
;
; RESTRICTIONS
;     file must contains zernikes from #4 to #22
;
; MODIFICATION HISTORY:
;     WRITTEN, BELMONT vincent, NOT, october 1999
;-
```

```
***** ordering zernikes in same order than active optics *****
*****          f1(*,*,0)  is focus          *****
*****          f1(*,*,1)  is coma           *****
*****          f1(*,*,2)  is spherical       *****
*****          f1(*,*,3)  is astigmatism     *****
```

```

;*****          f1(*,*,4)  is triangular coma          *****
;*****          f1(*,*,5)  is quadratic astigmatism    *****
;*****          f1(*,*,6)  is spherical astigmatism     *****
;*****          f1(*,*,7)  is (r^5,theta)               *****
;*****          f1(*,*,8)  is (r^5,3 theta)            *****
;*****          f1(*,*,9)  is (r^5,5 theta)            *****
:*****          f1(*,*,10) is spherical 6^th order     *****

```

```
function order_z,dt
```

```
f1=fltarr(2,2,11)
```

```

f1(*,0,0)=dt(*,0)
f1(*,0:1,1)=dt(*,3:4)
f1(*,0,2)=dt(*,7)
f1(*,0:1,3)=dt(*,1:2)
f1(*,0:1,4)=dt(*,5:6)
f1(*,0:1,5)=dt(*,10:11)
f1(*,0:1,6)=dt(*,8:9)
f1(*,0:1,7)=dt(*,12:13)
f1(*,0:1,8)=dt(*,14:15)
f1(*,0:1,9)=dt(*,16:17)
f1(*,0,10)=dt(*,18)

```

```
return,f1
END
```

```
;***** end of order_z *****
```

```
function extract_curv_data, f, sum
```

```
;***** extract Zernikes coeficients from output ef textfile *****
```

```

data0=read_strarr(f)
si=size(data0)
s=si(1)
cpt=0
i=0
for i=0,s-1 DO BEGIN
stri=data0(i)
byt=byte(stri)

```

```

IF ((byt(0) EQ 0) OR (strmid(stri,1,1) EQ 'Z') )THEN cpt=cpt+1 ELSE BEGIN
sepstring=str_sep(stri,string(byte([9,9])))
si=size(sepstring)
s2=si(1)
data0(i-cpt)=strcompress(sepstring(s2-1),/remove_all)
ENDELSE
ENDFOR

s=s-cpt
data=data0(0:s-1)
s=s/19
dat=fltarr(s+2,19)
FOR i=0,(s-1) DO BEGIN
dat(i,*)=rotate(data(19*i:19*i+18),4)
ENDFOR

;***** calculate average, and standard deviation for each zernikes *****

FOR i=0,18 DO BEGIN
M=moment(dat(0:(s-1),i))
dat(s,i)=M(0)
dat((s+1),i)=sqrt(M(1))
ENDFOR

;***** calculate quadratic sum of zernikes (total aberration) *****
;***** and its standard deviation *****

somme=fltarr(s)
sum=fltarr(2)
FOR j=0,s-1 DO BEGIN
FOR i=1,18 DO somme(j)=somme(j)+(dat(j,i))^2
somme(j) = SQRT(somme(j))
ENDFOR
M=moment(somme)
sum=M(0:1)
sum(1)=SQRT(sum(1))

;***** transform zernikes for (amplitude; angle) representation ****

dt_ord=order_z(dat(9:10,*))

dat2=fltarr(2,2,11)

```

```

FOR i=0,9 DO BEGIN
CASE 1 OF
(i EQ 0) OR (i EQ 2) OR (i EQ 10): dat2(*,0,i)= dt_ord(*,0,i)
(i EQ 1) OR (i EQ 3) OR (i EQ 4):BEGIN
rapport=-dt_ord(0,0,i)/dt_ord(0,1,i)
tetha = ATAN(rapport)
ampl=-dt_ord(0,0,i)/sin(tetha)
dat2(0,0,i)=ampl
dat2(0,1,i)=tetha
dat2(1,1,i)=(-dt_ord(0,1,i)*dt_ord(1,0,i)+dt_ord(0,0,i)*dt_ord(1,1,i))/\$
((dt_ord(0,0,i))^2+(dt_ord(0,1,i))^2)
dat2(1,0,i)=-((SIN(tetha)*dt_ord(1,0,i)-$
dt_ord(0,0,i)*COS(tetha)*dat2(1,1,i))/(SIN(tetha))^2)
END
(i EQ 5) OR (i EQ 6) OR (i EQ 7) OR (i EQ 8) OR (i EQ 9):BEGIN
rapport=-dt_ord(0,1,i)/dt_ord(0,0,i)
tetha = ATAN(rapport)
ampl=-dt_ord(0,1,i)/sin(tetha)
dat2(0,0,i)=ampl
dat2(0,1,i)=tetha
dat2(1,1,i)=(-dt_ord(0,0,i)*dt_ord(1,1,i)+dt_ord(0,1,i)*dt_ord(1,0,i))/\$
((dt_ord(0,0,i))^2+(dt_ord(0,1,i))^2)
dat2(1,0,i)=-((SIN(tetha)*dt_ord(1,1,i)-$
dt_ord(0,1,i)*COS(tetha)*dat2(1,1,i))/\$
(SIN(tetha))^2)
END
else:print,'if you read this sentence then you changed the source file...that is not
ENDCASE

ENDFOR

return,dat2
end

```

Appendix D

Beam splitter prism data and drawings

the Following pages shows the data and drawings for the beam splitter prism as they are given by ZEMAX:

- listing of surface data
- layout in 3 different views
- drawing of beam external rays in CCD plane for configuration 1 (direct path) and configuration 2 (indirect path)
- spot diagram in CCD plane for configuration 1 and 2